Journal of Sound and Vibration 363 (2016) 517–531

Contents lists available at ScienceDirect

Journal of Sound and Vibration

journal homepage: www.elsevier.com/locate/jsvi

Leveraging nonlinear saturation-based phenomena in an L-shaped vibration energy harvesting system

R.L. Harne [a,*], A. Sun [b], K.W. Wang [b]

[a] Department of Mechanical and Aerospace Engineering, The Ohio State University, Columbus, OH 43210, USA
[b] Department of Mechanical Engineering, University of Michigan, Ann Arbor, MI 48109, USA

ARTICLE INFO

Article history:
Received 3 February 2015
Received in revised form
27 October 2015
Accepted 9 November 2015
Handling Editor: M.P. Cartmell
Available online 21 November 2015

Keywords:
Vibration energy harvesting
Internal resonance
Saturation
L-shaped
Energy harvester

ABSTRACT

Trees exploit intriguing mechanisms such as multimodal frequency distributions and nonlinearities to distribute and dampen the aerodynamically-induced vibration energies to which they are subjected. In dynamical systems, these mechanisms are comparable to internal resonance phenomena. In recent years, researchers have harnessed strong nonlinearities, including internal resonance, to induce energetic dynamics that enhance performance of vibration energy harvesting systems. For trees, the internal resonance-like dynamics are evidently useful to dampen swaying motions in spite of the high variation associated with excitation and structural parameters. Yet for dynamic systems, studies show narrow operating regimes which exhibit internal resonance-based behaviors; this additionally suggests that the energetic dynamics may be susceptible to deactivation if stochastic inputs corrupt ideal excitation properties. To address these issues and to investigate whether the underlying motivation of exploiting internal resonance-induced saturation dynamics is truly justified, this research evaluates the opportunities enabled by exploiting nonlinear, multimodal motions in an L-shaped energy harvester platform. The system dynamics are probed analytically, numerically, and experimentally for comprehensive insights on the versatility of internal resonance-based behaviors for energy harvesting. It is found that although activating the high amplitude nonlinear dynamics to enhance power generation is robust to significant additive noise in the harmonic excitations, parameter sensitivities may pose practical challenges in application. Discussion is provided on means to address such concerns and on future strategies that may favorably exploit nonlinearity and multimodal dynamics for robust energy harvesting performance.

1. Introduction

The conversion of ambient vibration energies into electric power has recently been extensively investigated to realize a sustainable energy supply suitable for a wide range of engineered systems [1–3]. A common ambient vibration of high energy density is the swaying of engineered structures, such as tall buildings, due to aerodynamic and seismic excitations [4]. These same forces drive the oscillations of trees [5]. One may then hypothesize that the damping mechanisms which sustain trees may provide guidance towards the development of energy harvesting systems that efficiently convert the same motion- and wind-based excitations into electric power.

* Corresponding author.
E-mail address: harne.3@osu.edu (R.L. Harne).

http://dx.doi.org/10.1016/j.jsv.2015.11.017
0022-460X/

Trees leverage a variety of damping mechanisms for self-preservation when subjected to wind and seismic loads. Some features such as collision effects (e.g., branches rubbing) and aerodynamic phenomena (e.g., leaves flapping) contribute to dampen the swaying vibrations [6]. The remaining energies are dissipated via structural/material factors, about which several interesting hypotheses have been proposed. The nonlinear bending stiffness in numerous tree species led Miller [7] to examine the role of hardening and softening stiffnesses as means for trees to automatically shift the peak frequency of response away from the linear resonance to alleviate damaging stroke amplitudes under high excitation conditions. Spatz et al. [8] found that a tightly confined modal spacing in a Douglas fir was capable of providing substantial damping in the smaller branch oscillations due to efficient energy transfer from the swaying trunk; in the aerodynamically-loaded situation (in which case the branches are the excited members), this phenomenon was described as a means to suppress energy transfer to the trunk. Rodriguez et al. [9] proposed that a scaling law may exist to govern the transmission and dissipation of vibration amongst the trunk and various levels of branches via regularly spaced, but very dense, modal distributions. Later, Rodriguez et al. [10] tested the hypothesis via computational and experimental studies on walnut trees and found clear evidence that dense "mode groups" (such as dense clusters of natural frequencies around 1, 2, and 3 Hz), in contrast to continuously-distributed natural frequencies (such as a continuous spread of natural frequencies from 1 to 3 Hz), are key enablers of the vibration energy transfer and dissipation mechanisms utilized by trees under mechanical loading situations.

Considering such modal spacings in greater detail, Theckes et al. [11] showed that the multimodal dynamics of trees provides for an appreciably enhanced energy dissipation when the hierarchical composition follows certain scales amongst the modal natural frequencies, damping ratios, and masses; for example, a 1:2 proportionality between the two lowest order mode natural frequencies (i.e., $\omega_2 \approx 2\omega_1$, a 1:2 internal resonance) clearly promotes the substantial damping effects when the swaying displacements become large. A thorough and recent review of the structural/material damping strategies of trees may also be found in Ref. [12].

The themes of these studies suggest that nonlinearity and multimodality play critical roles in the dynamical behaviors of trees for the purposes of structural damping. Indeed, the occurrence of an internal resonance suggests that some trees exploit particularly unique energy transfer characteristics. For different purposes altogether, energy harvesting structures are designed to efficiently absorb and electrically dissipate the vibrations to which they are subjected. While to date there have been numerous energy harvesting investigations focused on nonlinearity or multimodality as individual features [13–15], there are few that have considered exploiting both phenomena concurrently to improve energy conversion. Wu et al. [16] showed a broadening of nonlinear "resonant" bandwidths was achieved by employing a two degree-of-freedom (DOF) structure having internal magnetic interactions to induce nonlinear restoring forces. Harne et al. [17] and Wu et al. [18] discovered that the incorporation of bistability – that is, the existence of two statically stable states – in two DOF energy harvesters could be leveraged for enhanced performance. Litak [19] examined two electrically-coupled piezomagnetoelastic harvesters and showed that additive random excitation could assist in activating the bistable "snap-through" behaviors in spite of mistuning between the structures. Karimpour and Eftekari [20] and Chen and Jiang [21] analytically explored the 1:1 and 1:2 internal resonances as bases for inducing large amplitude motions in alternative vibration modes of monostable energy harvesting devices. Nonlinearity and multimodality have also attracted recent attention as tools to advance the performance of vibration absorption [22], vibration isolation [23,24], and sensing systems [25].

In spite of the active explorations on the potential for nonlinearity and multimodality to enhance energy harvesting system performance, there are several important questions which remain to be answered, particularly regarding how these two features are best integrated and exploited via internal resonance. For instance, a prime motivation is to "broaden" the operating frequency bandwidth of the vibration energy harvester by harnessing the large amplitude behaviors near the lower order natural frequency induced in consequence to excitations at approximately twice this frequency via 1:2 internal resonance (the saturation phenomenon). On the other hand, since the common piezoelectric and electromagnetic electromechanical conversion strategies generate an amplitude of harmonic current flow in proportion to the frequency of the excitations, activating nonlinear motions at a lower frequency may not provide advantage. The prior research efforts have not addressed whether the underlying motivation of exploiting internal resonance-induced saturation features is truly justified. Another concern is related to the robustness of activating the large amplitude dynamics when design and/or excitation parameters are known inexactly or undesirably change over time. Established studies on 1:2 internal resonance [26–28] have shown that there can be severely limited operating and design regimes over which large amplitude motions are induced. Such observations are obviously a practical concern for vibration energy harvesting systems unless excessive control is available for device fabrication and the harmonic excitation parameters are sufficiently static. Additionally, while trees are occasionally subjected to harmonic excitations related to seismic or flutter-type phenomena, by and large the excitation form is stochastic [29]. Likewise, energy harvesters may be operated in strongly stochastic environments or be under excitations which vary in the degree to which an individual frequency dominates above a background noise. Although internal resonance shows beneficial results in consequence to purely harmonic excitations on energy harvesters [20,21], the robustness of the phenomena when the significance of the harmonic contribution is reduced is not well understood, thus potentially compromising the viability of leveraging the nonlinear behaviors for energy harvesting enhancements. Indeed, as it relates to purely mechanical systems, the investigations conducted to characterize the stochastic sensitivity of nonlinearly coupled structures possessing 1:2 internal resonance show that the large amplitude dynamic effects may lose their stability due to the stochastic perturbations [30–32].

This research seeks to address these important questions by investigating a prototypical, monostable energy harvesting platform which exploits the 1:2 internal resonance. The justification for utilizing the phenomenon and the sensitivities

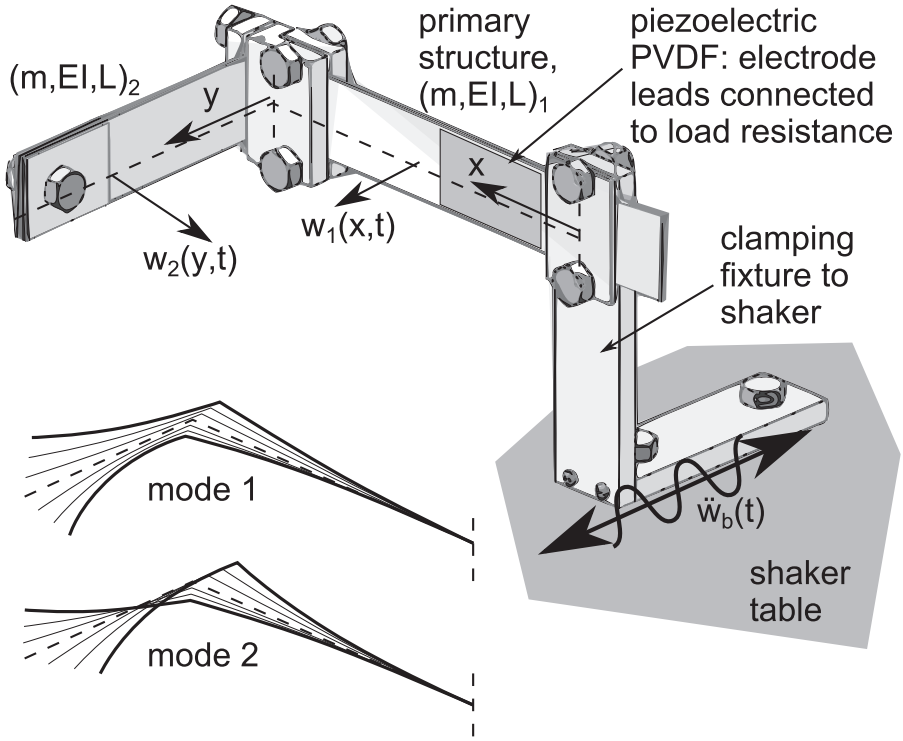

Fig. 1. Schematic of the experimentally fabricated L-shaped energy harvester platform considered for its ability to exploit the 1:2 internal resonance for energy harvesting enhancements. At bottom left, the first two modal behaviors are illustrated.

encountered in the process are considered in detail. Examinations of both pure harmonic and mixed harmonic and stochastic excitations are undertaken to determine the robustness of the phenomena when an ideal periodic forcing may no longer be available from the net ambient vibration. The use of models and experiments helps to thoroughly support the conclusions. The following sections present these investigations to detail the opportunities and limitations encountered when simultaneously harnessing strong nonlinearities and multimodal dynamics via the 1:2 internal resonance in an L-shaped vibration energy harvesting system.

2. Energy harvesting platform overview

The design of the energy harvesting platform considered in this research is based upon a prototypical structure previously considered by a variety of researchers. The structure leverages a 1:2 proportionality of linear mode natural frequencies which is readily achieved by design and also induces strong nonlinear phenomena featuring large displacements, favorable for energy harvesting objectives. The platform is shown in Fig. 1 and consists of two beam-mass sub-systems that are clamped together in the shape of the letter L. The other end of the primary structure is clamped to a fixture which moves along with the motions of an electrodynamic shaker table representative of an ambient vibration resource. This is the archetypal experimental platform originally considered by Haddow et al. [26] and Balachandran and Nayfeh [27], who uncovered and examined the occurrence of unusually strong nonlinear dynamics in this otherwise straightforward structural composition.

For the platform as studied here, piezoelectric PVDF patches are attached on both sides of the primary, excited beam near the end which is clamped to the exciting base. The bonds between PVDF and the spring steel beam are made by cyanoacrylate. The PVDF patches are attached such that the electrode leads are combined in a series circuit with a load resistance to maximize the charge extraction from beam motions. In this research, the beams are composed from spring steel strips of 25.4 mm width and 0.508 mm thickness and are cut to the lengths reported in Tables 1 and 2, while the attached lumped masses are custom-machined aluminum blocks sized so as to facilitate the 1:2 proportionality of linear mode natural frequencies following further design adjustments. These latter adjustments include minor, iterative repositioning of the aluminum blocks along the lengths of the beams to precisely achieve the 1:2 proportionality of the natural frequencies. Erturk et al. [33] considered a companion design to this platform, where the energy harvesting sub-systems were piezoelectric unimorphs such that piezoelectric material covered one full surface of each sub-structural beam. For the experimentation undertaken in this research, the acceleration of the controlled APS Dynamics 400 shaker table is measured using a PCB 352 C33 accelerometer, while the displacement and velocity of the primary structure at the free end, $w_1(L_1,t)$, are measured

Table 1
Platform design yielding $\omega_2/\omega_1 = 2.009$.

m_1, g	EI_1, N m^2	L_1, mm	ζ_1	$\omega_1/2\pi$, Hz
122	0.886	126.8	0.003	11.4589
m_2, g	EI_2, N m^2	L_2, mm	ζ_2	$\omega_2/2\pi$, Hz
61.0	0.145	72.8	0.003	23.0290

Table 2
Platform design yielding $\omega_2/\omega_1 = 1.998$.

m_1, g	EI_1, N m^2	L_1, mm	ζ_1	$\omega_1/2\pi$, Hz
120	0.886	127.0	0.003	11.4331
m_2, g	EI_2, N m^2	L_2, mm	ζ_2	$\omega_2/2\pi$, Hz
61.0	0.145	73.5	0.003	22.8394

using a Polytec OFV 303 laser interferometer and OFV 3001S controller. Throughout this study, the transduced voltages from the piezoelectric PVDF patches are measured across a 5.4 MΩ load resistance.

For the platform shown in Fig. 1, the two beam-mass sub-systems are coupled parametrically. In other words, in the governing equations of motion the coupling appears to change parameter coefficients related to the states of each sub-system. Another result of the boundary condition between the sub-systems is that the excitation similarly influences system parameter values. Parametric coupling and parametric excitation of dynamical systems are well-known to be sources for strong nonlinearity [34,35] and here these factors are exploited to appropriately tune and couple the sub-systems for exciting a 1:2 internal resonance in the monostable energy harvester platform. The saturation phenomenon, to be explored in detail in later sections of this study, is a feature of internal resonance which additionally requires the presence of a quadratic nonlinearity [36]. In the platform considered in this research, the quadratic nonlinearity is induced due to the parametric coupling.

3. Rationale for exploiting internal resonance and saturation in an energy harvesting system

The focus of this research is on the scenario in which the harmonic excitations are at an absolute frequency Ω around the second mode natural frequency ω_2. This is because the saturation phenomenon may be exploited for the purpose of hypothetically enhancing the resulting power generation due to activating large amplitude motions. By utilizing a 1:2 internally resonant platform (i.e., $\omega_2 \approx 2\omega_1$) including a quadratic nonlinearity, large strains may be induced in the structure around the lower order natural frequency ω_1 when the system is excited at a frequency near ω_2. Thus, the saturation phenomenon triggers large fundamental mode motions near frequency ω_1, even though the excitations are near frequency ω_2 which for small levels of excitation only cause displacements associated with the second mode shape (see Fig. 1 for the corresponding mode shapes).

It is known that for excitations of frequency Ω near ω_1, the structure will undergo dynamics having greater contribution from fundamental modal motions, whether activated in linear [33] or nonlinear [26] regimes, while a smaller proportion of the energy will diffuse to the second harmonic of the excitation frequency [36,37], which is approximately ω_2 ($2\Omega \approx \omega_2$). These dynamical behaviors are not particularly advantageous in the context of vibration energy harvesting because there is no resulting amplification of displacements, but instead only a diffusion of the harmonic energy to higher frequency vibrations characterized by smaller amplitude motions. Thus, if there is a feature to intelligently exploit for the L-shaped, internally resonant energy harvesting system, it is related to saturation phenomenon occurring for harmonic excitations with frequency Ω near ω_2. Only under this condition is it possible to trigger larger amplitude dynamics than are otherwise achievable with a linear structure. The net result of this approach is an energy harvesting platform possessing a broad bandwidth of frequencies at which it is sensitive to undergo large amplitude motions and, hence, induce large power across an external circuit load.

Fig. 2 exemplifies the benefits which may be harvested, showing experimentally measured results that illustrate the saturation phenomenon. The measurements are taken using the system described in Section 2 and with the design parameters given in Table 1. Fig. 2(a) plots the fast Fourier transform (fft) amplitudes of the primary beam-mass structure displacements which are proportional to frequencies $\Omega/2 \approx \omega_1$ and $\Omega \approx \omega_2$. The results are shown for all of the coexistent responses that are induced when the structure is excited with frequency Ω near the second mode natural frequency ω_2. All of the stable dynamics are captured in the experiment by very slowly sweeping the amplitude of excitation up and down in level with a swept speed of 0.006 m/s^3. Around an excitation amplitude of 1.4 m/s^2 in the upwards sweep, the saturation phenomena occurs and the amplitude of the response proportional to the excitation frequency $\Omega \approx \omega_2$ is observed to flatten for further increase in the excitation amplitude (i.e., the response proportional to $\Omega \approx \omega_2$ saturates).

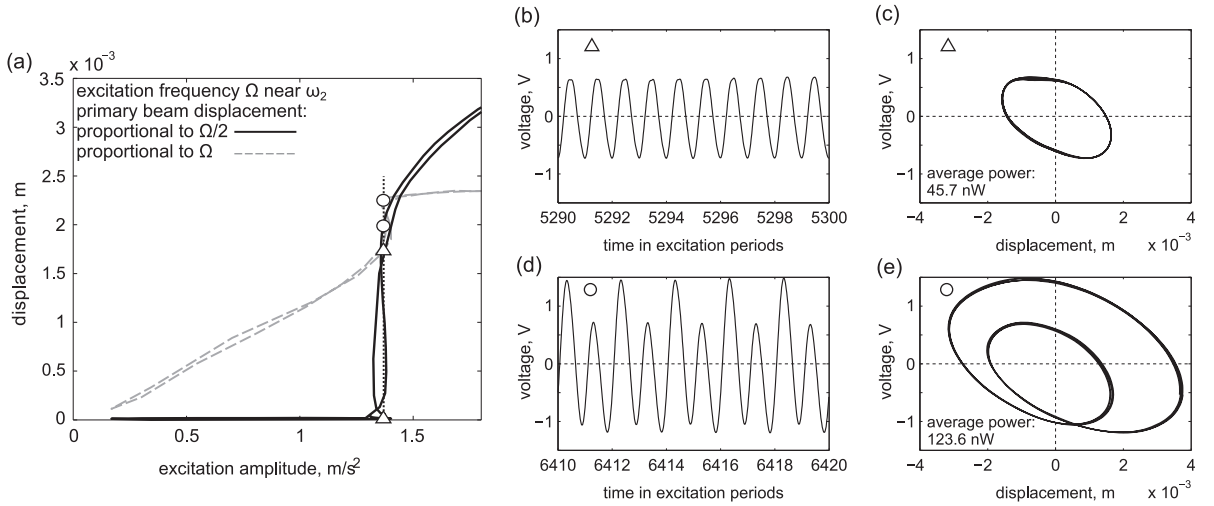

Fig. 2. Saturation in the 1:2 internally resonant energy harvesting platform. (a) Experimentally measured displacement of primary beam-mass structure for excitations at frequency 22.89 Hz which is near to the second mode natural frequency ω_2. Very slow forward and backward sweeps in excitation amplitude are conducted to capture all responses. The symbols indicate the beam response amplitudes proportional to frequencies ω_1 and ω_2 for the two coexistent responses at excitation 1.4 m/s^2. (b–e) show the corresponding plots of voltage in time, and displacement–voltage phase plane for the response conditions indicated by the symbols in (a).

Near this critical excitation level, two coexistent responses are identified, which have unique pairs of response amplitudes proportional to the frequencies $\Omega/2 \approx \omega_1$ and $\Omega \approx \omega_2$. Each pair is indicated by a symbol in Fig. 2(a). In Fig. 2(b), the time series of the measured voltage across a 5.4 MΩ resistor is shown for the linear response when no contribution from the frequency $\Omega/2 \approx \omega_1$ is present; Fig. 2(c) shows the corresponding phase portrait in the displacement–voltage plane. In Fig. 2 (d,e) are shown the corresponding results for the saturated dynamics which activate both frequencies. In spite of the diffusion of the harmonic energy away from the excitation frequency $\Omega \approx \omega_2$ to the lower frequency $\Omega/2 \approx \omega_1$, the average power that is measured across the load resistance is increased by approximately 2.7 times for the nonlinear response due to the fact that the motions proportional to frequency $\Omega/2 \approx \omega_1$ are so large in amplitude. It is particularly important to confirm that this nonlinear phenomena increases the average power because piezoelectrically-induced voltage is a velocity-proportional phenomenon [2], which for harmonic excitation is increased in amplitude as frequency increases (all else remaining the same). Thus, an increase in the average power shows that even though the energy harvesting platform diffuses energy to the lower frequency dynamics via saturation, the large amplitude of the resulting motions is such that the oscillation frequency reduction does not prevent the enhancement of power generation.

The experimental results presented in Fig. 2 are key evidence that there are particular performance improvements to be realized by intelligently utilizing the saturation phenomenon in a 1:2 internally resonant energy harvesting platform. This provides important justification for the original research motivation. On the other hand, a look at further results is instructive before undertaking the following study since several factors and sensitivities are involved in regards to triggering the large amplitude dynamics. Fig. 3 presents measurements of the saturation-related behaviors as the excitation frequency is very slowly increased and then decreased using a swept speed of 0.004 Hz/s while using an excitation amplitude of 2.33 m/s^2. For the design of the harvester platform employed in this experiment, the absolute frequency of ω_2 is 22.84 Hz. As Fig. 3(a) makes clear, a significant increase in the system response may be induced due to the saturation of the responses proportional to the second mode natural frequency $\Omega \approx \omega_2$. In a comparable manner as found in Fig. 2, Fig. 3(b–e) show the time series and phase portraits of the voltage across a 5.4 MΩ resistor for the pair of coexisting responses which occur for an excitation frequency $\Omega = 22.31$ Hz where the contributions of responses at both frequencies $\Omega \approx \omega_2$ and $\Omega/2 \approx \omega_1$ are apparent. Fig. 3(e) shows that the average power more than doubles for the saturated response such that the motions of frequency $\Omega/2 \approx \omega_1$ predominate. Fig. 3(d) also plainly indicates that the primary period of oscillation in the harvester platform is twice the excitation period, thus the major frequency of oscillation is $\Omega/2 \approx \omega_1$.

On the other hand, Fig. 3(a) exemplifies the large sensitivity of the phenomenon in terms of change in the harmonic frequency of excitation. Even for the large excitation level of 2.33 m/s^2 (relative to the level of many ambient vibrations [38]), the magnitude of the frequency bandwidth spanning the beneficial activation of the saturation features is only about 0.75 Hz. Given that exciting vibrations may readily deviate from one pure tonal frequency, the fine sensitivity observed here suggests that the useful power-amplifying phenomenon may not be particularly robust for this structural platform. Moreover, given that ambient vibrations commonly contain a contribution of stochastic (i.e., non-deterministic) motions, one may hypothesize how the results of Fig. 3(a) might change if the driving signal was no longer a pure tone. Although the benefits of activating saturation in the 1:2 internally resonant, L-shaped, energy harvesting platform include an obvious amplification of the generated power – thereby justifying the basis of the study – the robustness and sensitivities of the phenomenon are uncertain and are therefore evaluated in the following sections.

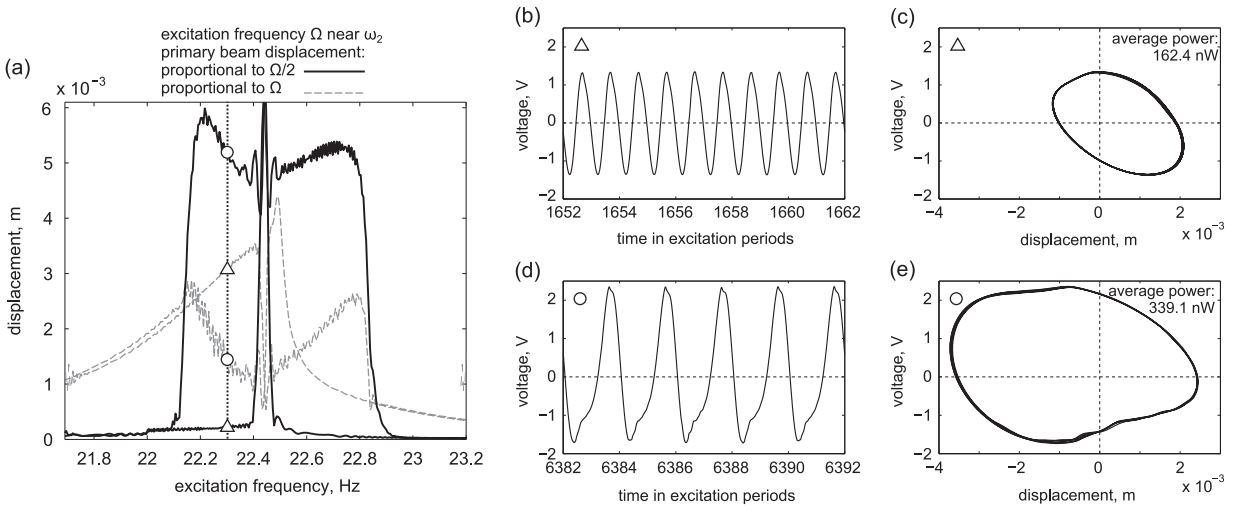

Fig. 3. Saturation as observed due to change in excitation frequency. (a) Experimentally measured displacement of primary beam-mass structure for excitations with amplitude 2.33 m/s^2 near to the second mode natural frequency ω_2. Very slow forward and backward sweeps in excitation frequency are conducted to capture all of the potential responses. The symbols indicate the beam response amplitudes proportional to frequencies ω_1 and ω_2 for the two coexistent responses at excitation frequency 22.31 Hz. (b–e) show the corresponding plots of voltage in time, and displacement–voltage phase plane for the points as indicated by the symbols.

4. Model formulation

4.1. Governing equations of motion

To help assess these factors as related to the L-shaped energy harvesting platform, this research employs an established model of the mechanical composition of the system. Haddow et al. [26] previously devised and experimentally validated the model of the structure when excited by single-frequency harmonic base motions, while Balachandran and Nayfeh [27] and Nayfeh et al. [39] studied the resulting nonlinear dynamics particularly in regards to the intriguing Hopf bifurcation which may occur. These works used a model which neglected the electromechanical constituents based upon the small static and dynamic influences of the transduction methods (surface-bonded strain gauges in all cases). On the other hand, Erturk et al. [33] examined the linear responses of the structure when it was composed using two, piezoelectric PZT-5A unimorphs attached at a right angle. Due to the significance of the piezoelectric material with regard to the net electroelastic properties, the fully coupled electromechanical dynamics were considered and examined in the context of energy harvesting under linear vibrations [33]. In this study, the piezoelectric PVDF material that is surface-bonded to the primary structure presents a small electroelastic influence to the resulting system dynamics due to the flexibility of the material when compared to the spring steel beam sub-structure and because of the weaker electromechanical coupling inherent in piezoelectric PVDF. Consequently, it is sufficient to employ and examine the energy harvesting platform shown in Fig. 1 using the previous model composition of Haddow et al [26]. The use of this prior model provides means to quantitatively and qualitatively compare results of the modeled structural dynamics with corresponding measurements; a qualitative comparison is also possible between the measured voltage across the external load resistance and the modeled primary structure velocity, since the transduced voltage is proportional to the velocity of the beam to which the piezoelectric PVDF is attached. A brief summary of the model development is provided below, while Ref. [26] presents the full details.

The beams are modeled using Euler–Bernoulli assumptions: shear deformation and rotational inertia are omitted and the uniaxial strain distribution varies linearly away from the (here, central) neutral axis of deformation. The end masses are assumed to have negligible rotational inertia. The total kinetic and potential energies are derived and Lagrange's method is employed to determine the governing equations of motion. The kinetic energies of each sub-system are expressed by assuming the masses of each sub-system are representative of a portion of each beam mass, according to equivalent lumped-parameter assumptions [40], and the respective end mass. Therefore, the total kinetic energy T is expressed by

$$T=\frac{1}{2}m_1\left[[\dot{w}_b(t)+\dot{w}_1(L_1,t)]^2+\frac{d}{dt}\left\{\frac{1}{2}\int_0^{L_1}\left[\frac{\partial w_1(x,t)}{\partial x}\right]^2 dx\right\}^2\right]$$
$$+\frac{1}{2}m_2\left[\left(\dot{w}_b(t)+\dot{w}_1(L_1,t)-\frac{d}{dt}\left\{\frac{1}{2}\int_0^{L_2}\left[\frac{\partial w_2(y,t)}{\partial y}\right]^2 dy\right\}\right)^2\right.$$
$$\left.+\left(\dot{w}_2(L_2,t)+\frac{d}{dt}\left\{\frac{1}{2}\int_0^{L_1}\left[\frac{\partial w_1(x,t)}{\partial x}\right]^2 dx\right\}\right)^2\right] \quad (1)$$

where $\ddot{w}_b(t) = A\ \cos\left[\Omega t\right]$ is the harmonic acceleration of the base; $w_1(x,t)$ and $w_2(y,t)$ are the transverse motions of the sub-systems 1 and 2 masses, respectively; and $L_{1,2}$ are the respective sub-structural beam lengths. The overdot is used to denote the time derivative. The sole source of the nonlinearity in the system results from the axial motions of masses 1 and 2, $m_{1,2}$ according to the L-shaped structural fabrication. In the experimental system, the weak electro-elastic effects of the piezoelectric PVDF patches on the structural responses of the beam-mass sub-systems implies that the voltage $V(t)$ measured across the load resistance R_L is related to the velocity of the primary beam according to

$$V(t) = -\theta \int_0^{L_p} \frac{\partial^3 w_1(x,t)}{\partial x^2 \partial t} \mathrm{d}x$$

where L_p is the length of the piezoelectric PVDF patches and θ is a coefficient related to the capacitance of the piezoelectric materials, the resistive load, the electromechanical coupling coefficient, and the lowest order short-circuit natural frequency of the system.

The total potential energy is

$$U = \frac{1}{2}\left[EI_1 \int_0^{L_1} \left(\frac{\partial^2 w_1}{\partial x^2}\right)^2 \mathrm{d}x + EI_2 \int_0^{L_2} \left(\frac{\partial^2 w_2}{\partial y^2}\right)^2 \mathrm{d}y\right] \tag{2}$$

Before applying Lagrange's method, the displacements $w_1(x,t)$ and $w_2(y,t)$ are assumed to be a combination of the linear mode shapes, expressed using polynomials differentiable in x up to the required order [26], that have amplitudes $u_i(t)$, $(i=1,2)$ (the generalized coordinates). Applying Lagrange's method and retaining terms of order two and less yields the governing equations [26]

$$\begin{bmatrix} \ddot{u}_1 \\ \ddot{u}_2 \end{bmatrix} + 2\varepsilon \begin{bmatrix} \mu_1 & 0 \\ 0 & \mu_2 \end{bmatrix} \begin{bmatrix} \dot{u}_1 \\ \dot{u}_2 \end{bmatrix} + \begin{bmatrix} \tilde{\omega}_1^2 & 0 \\ 0 & \tilde{\omega}_2^2 \end{bmatrix} \begin{bmatrix} u_1 \\ u_2 \end{bmatrix}$$
$$+\varepsilon \begin{bmatrix} X_{11} & X_{12} & X_{13} \\ X_{21} & X_{22} & X_{23} \end{bmatrix} \begin{bmatrix} \dot{u}_1^2 \\ \dot{u}_1\dot{u}_2 \\ \dot{u}_2^2 \end{bmatrix} + \varepsilon \begin{bmatrix} Y_{11} & Y_{12} & Y_{13} & Y_{14} \\ Y_{21} & Y_{22} & Y_{23} & Y_{24} \end{bmatrix} \begin{bmatrix} u_1\ddot{u}_1 \\ u_1\ddot{u}_2 \\ u_2\ddot{u}_1 \\ u_2\ddot{u}_2 \end{bmatrix}$$
$$+2\varepsilon F\tilde{\Omega}\ \cos\ \tilde{\Omega}\tau \begin{bmatrix} Z_{11} & Z_{12} \\ Z_{21} & Z_{22} \end{bmatrix} \begin{bmatrix} u_1 \\ u_2 \end{bmatrix} = 2F \begin{bmatrix} K_1 \\ K_2 \end{bmatrix} \cos\ \tilde{\Omega}\tau \tag{3}$$

In Eq. (3), $\varepsilon << 1$ (here, $\varepsilon = 0.01$) is a parameter to denote that the damping (with coefficients μ), nonlinear parametric coupling (coefficients X and Y), and level of parametric excitation (coefficients Z) contribute small influences with respect to the underlying, base-excited linear dynamics. The nondimensional natural frequencies are $\tilde{\omega}_{1,2}$ and the nondimensional time is τ, while the base excitation (shaker motion) is assumed to be harmonic using $w_b(\tau) = \varepsilon L_1 F\ \cos\ \tilde{\Omega}\tau$. The interested reader is referred to Ref. [26] for explicit definition of all coefficients in Eq. (3).

In this study, Eq. (3) is investigated using numerical simulations to determine the structural dynamics when excited by harmonic motions as well as by white Gaussian noise. To include the contribution of noise, the final two terms of Eq. (3) are modified as follows

$$\cdots + \varepsilon\left[2F\tilde{\Omega}\ \cos\ \tilde{\Omega}\tau + n_a(\tau)\right] \begin{bmatrix} Z_{11} & Z_{12} \\ Z_{21} & Z_{22} \end{bmatrix} \begin{bmatrix} u_1 \\ u_2 \end{bmatrix} = \left[2F\ \cos\ \tilde{\Omega}\tau + n_a(\tau)\right] \begin{bmatrix} K_1 \\ K_2 \end{bmatrix} \tag{4}$$

where $n_a(\tau)$ is a zero-mean, random noise having normal distribution and standard deviation σ_n determined from

$$SNR = 20\log_{10}\left(\frac{F}{\sigma_n}\right) \tag{5}$$

The signal-to-noise ratio (SNR), expressed using dB, determines the significance of the harmonic drive with respect to the stochastic contribution. Thus, Eq. (3) with the modified excitations given by Eq. (4) is employed in the following simulations.

4.2. Method for solving the governing equations of motion

The steady-state structural responses of the L-shaped energy harvesting platform may be approximately determined by an analytical approach when the excitations are pure sinusoids, $n_a \to 0$ (thus, $SNR \to \infty$ dB). The advantages of such a strategy are that it provides a direct means to predict the steady-state dynamical behaviors for a given set of excitations and system parameters at a small fraction of the computational cost of numerical simulations. Here, the method of multiple scales (MMS) is employed to solve Eq. (3). Following the approach by Haddow et al. [26], the nondimensional amplitudes u_i, $(i=1,2)$ proportional to the two lowest order modes are expanded in an infinite power series in terms of the small parameter ε:

$$u_i(\tau;\varepsilon) = u_{i0}(T_0,T_1,T_2,\cdots) + \varepsilon u_{i1}(T_0,T_1,T_2,\cdots) + \varepsilon^2 u_{i2}(T_0,T_1,T_2,\cdots) + \cdots \tag{6}$$

The first subscript i for each expanded term $u_{i(0,1,2,\cdots)}$ is 1 or 2 as relates to the generalized displacement amplitude of interest, and the T_j $(j=0,1,2,\cdots)$ are rescaled times given by $T_0=\varepsilon^0\tau$, $T_1=\varepsilon^1\tau$, $T_2=\varepsilon^2\tau$, and so on. Using MMS, the assumed solutions for the generalized displacement amplitudes u_i, $(i=1,2)$ in Eq. (6) are substituted into Eq. (3) and coefficients sharing a common order of the parameter ε are grouped. The resulting coefficients sharing a common ε are then set equal to zero, which yields a series of differential equations. Following this procedure, one sequentially solves the resulting equations until a satisfactory degree of accuracy is achieved. Since steady-state excitations are the primary interest in this study and based upon the nonlinear dynamical phenomena under consideration, only the first order expansion is employed: $u_i \approx u_{i0}(T_0,T_1)+\varepsilon u_{i1}(T_0,T_1)$. Higher order expansions are typically required for a useful degree of accuracy regarding transient dynamics.

In the event that the nondimensional frequency of excitation $\tilde{\Omega}$ is near the nondimensional second mode natural frequency $\tilde{\omega}_2$, the application of MMS to Eq. (3) yields a set of nonlinear, algebraic equations which are solved for two cases representing (i) the linear vibrations and (ii) when the saturation phenomenon is activated, based upon the amplitude of the oscillations. The reader is referred to the prior model developments [26] for complete details on the approximate solution strategy of MMS in the context of this internally resonant structural system. The results presented hereafter for the steady-state displacements and velocities of the energy harvesting platform are derived from this model.

Using this analytical foundation [26], two particularly relevant cases may be identified for close examination in this study for which (i) a switch occurs between the linear and nonlinear dynamic regimes and (ii) when the coexistence of responses may be induced in the nonlinear regime. Under condition (i), a critical amplitude of the harmonic base acceleration, $|\ddot{w}_b|$, may be derived to be

$$A_i = \frac{2\varepsilon^2\tilde{\omega}_2\tilde{\Omega}^2 EI_1}{m_1L_1^2C_1K_1}\sqrt{\left[\sigma_2^2+\mu_2^2\right]^2\left[(\sigma_1+\sigma_2)^2+4\mu_1^2\right]} \tag{7}$$

where $\sigma_2=\left(\tilde{\Omega}-\tilde{\omega}_2\right)/\varepsilon$ is the scaled nearness of the excitation frequency $\tilde{\Omega}$ to the second mode natural frequency $\tilde{\omega}_2$; $\sigma_1=(\tilde{\omega}_2-2\tilde{\omega}_1)/\varepsilon$ is the scaled nearness to an exact 1:2 internal resonance condition; and coefficients C_1 and K_1 are nondimensional values related to structural composition that are given in the appendix of Ref. [26]. Substituting in units, the only dimensioned constituents of Eq. (7) are EI_1, m_1, and L_1, which yields a dimension of m/s^2. Therefore, for harmonic base acceleration amplitudes A greater than A_i, the linear dynamic regime that produces motions proportional only to $\tilde{\Omega}\approx\tilde{\omega}_2$ is no longer stable: a pitchfork bifurcation occurs and the saturation phenomenon is thereafter triggered. In other words, only the strongly nonlinear dynamics are possible for $A>A_i$.

Regarding condition (ii), when the additional inequality $\sigma_2(\sigma_1+\sigma_2)-2\mu_1\mu_2>0$ is satisfied – which relates several nondimensional deviations amongst frequency relationships and damping parameters – the coexistence of the linear and nonlinear dynamic regimes will occur so long as

$$A_i > A > A_{ii} = \frac{2\varepsilon^2\tilde{\omega}_2\tilde{\Omega}^2 EI_1}{m_1L_1^2C_1K_1}\left|2\mu_1\sigma_2+\mu_2(\sigma_1+\sigma_2)\right| \tag{8}$$

Thus, for excitation conditions satisfying the inequality in Eq. (8), it is *possible* to activate the large amplitude saturated dynamics in the L-shaped energy harvester. Determining the likelihood of triggering these responses is the subject of basin of attraction mapping, which assesses the parametric and initial condition sensitivities of the system. Finally, when $A<A_{ii}$ only the linear dynamic regime is observed. The following section investigates these criteria for the L-shaped energy harvesting system as fabricated in the laboratory to understand the sensitivities of triggering the saturation phenomenon that is beneficial for enhancing power generation. The section thereafter explores the steady-state and noise-excited responses via the analytical model, numerical simulations, and experimentation.

5. Sensitivity to variation in pure harmonic excitation conditions and design parameters

The criteria given by Eqs. (7) and (8) are first explored to closely detail the sensitivity observed experimentally via Fig. 3 (a) pertaining to the successful triggering of the saturation phenomenon to amplify the generated power. Fig. 4 plots the criteria of required base acceleration to induce saturation when computed for one configuration of the L-shaped energy harvesting platform using the design parameters presented in Table 1. The results are shown using the parameter plane of dimensional excitation frequency Ω and logarithm of the damping ratio, $\zeta_i=\varepsilon\mu_i/\omega_i$. Table 1 provides the natural frequencies of this configuration which yields a ratio of second to first natural frequencies of 2.009. In the axis of damping ratio in Fig. 4, the damping ratios of both sub-systems are assumed to be identical, which was the case in the experimental platform.

The surfaces plotted in Fig. 4 are the range of excitation frequencies, damping ratios, and base acceleration amplitudes that exactly define the criteria of Eqs. (7) and (8). Thus for a given excitation frequency and damping ratio, base acceleration amplitudes *greater* than the surfaces will induce an enhancement of power generation by the saturation phenomena. Coexistence of the low amplitude linear dynamic regime and the saturated regime occurs for excitation and system parameters representing the volume between the darker shaded surface and the top light shaded surface. The logarithmic scale of base acceleration amplitude and the linear scale in frequency suggest that a severe sensitivity to activating the high

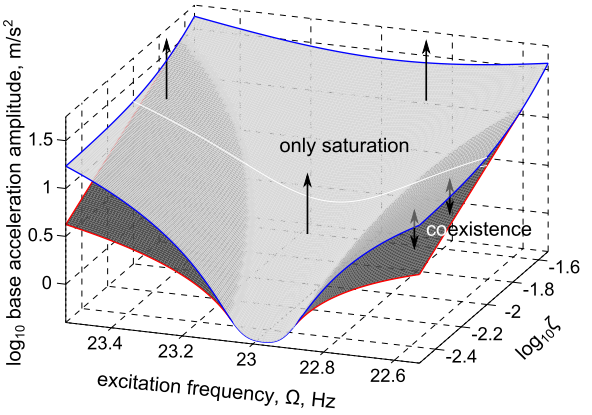

Fig. 4. Criteria for activating the saturated dynamics to amplify the power generation. Parameter plane of excitation frequency and damping ratio (equal for both sub-systems). Here $\omega_2/\omega_1 = 2.009$ and $\omega_2/2\pi = 23.03$ Hz.

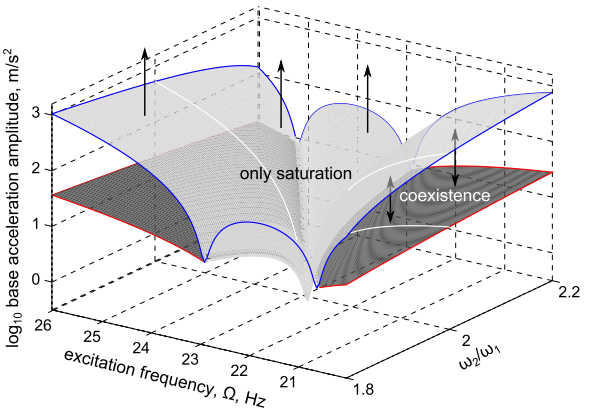

Fig. 5. Criteria for activating the saturated dynamics to amplify the power generation. Parameter plane of excitation frequency and ratio of natural frequencies. Here $\zeta_{1,2} = 0.003$ and $\omega_2/2\pi = 23.03$ Hz.

amplitude responses may be encountered. As is clear, only a very narrow band of frequencies, and at the lowest of damping ratios, allows for small amplitudes of harmonic excitation to activate the saturation phenomenon.

The smallest value of damping ratio presented in Fig. 4 corresponds to the specific design of the experimental system ($\zeta_{1,2} = 0.003$). The white lines in Fig. 4 illustrate the critical parameters required to activate saturation when damping ratio is $\zeta_{1,2} = 0.01$. Whereas a minimum of base acceleration of 0.43 m/s^2 is needed to trigger saturation for the experimentally realized design of this platform, if the damping ratio is increased to $\zeta_{1,2} = 0.01$, the required harmonic excitation increases substantially to 3.11 m/s^2. Although the amplitude of harmonic vibrations is strongly dependent upon the context of the application, many ambient motions of structural or mechanical systems (e.g., bridge components) have harmonic frequency amplitudes less than 1 m/s^2 [38]. Thus, for the L-shaped energy harvesting system, it appears that care must be taken to minimize the inherent damping mechanisms to effectively trigger saturation for enhancing the power generation.

Another look at the criteria is useful in the parameter plane of excitation frequency and the ratio of the natural frequencies ω_2/ω_1. These results are plotted in Fig. 5. As seen in the figure, only for a narrow band of natural frequency ratios very close to 2 (highlighted using the white lines) are the benefits of enhanced power generation possible via the saturation phenomenon for practical levels of base acceleration. Outside of this design regime, the required base acceleration grows substantially. Interestingly, the saturated dynamic regime may still be activated far away from the design condition of $\omega_2/\omega_1 = 2$ and $\Omega \approx \omega_2$ so long as the amplitude of the harmonic acceleration is sufficiently large to counterbalance the adverse influences of non-ideal parameters.

As is made clear via the results presented in Figs. 4 and 5, for pure harmonic excitation there may be non-trivial sensitivities encountered when one attempts to leverage the benefits of saturation in the L-shaped energy harvesting system for the purposes of enhancing power generation. Yet, high sensitivity to design may not be a considerable concern in some instances. For instance, the excitation may in fact be purely harmonic and carefully-monitored fabrication procedures could lead to structures having exact specifications.

On the other hand, ambient vibrations, even if possessing a strong tonal harmonic frequency, are oftentimes time-varying and moderately diffused in terms of spectral content. Depending upon the time-varying nature of the motions, effective models of these factors could consider the excitation to either be a tone with a high background noise or a

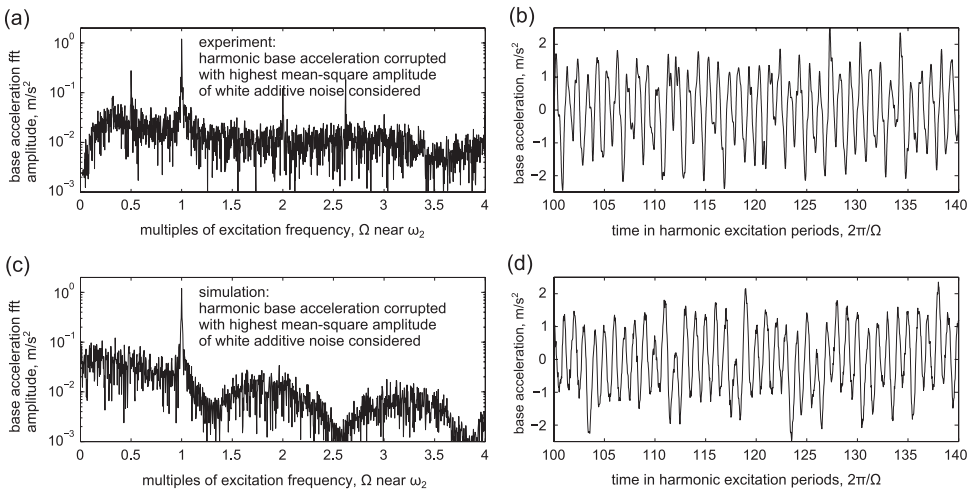

Fig. 6. Comparison of −6 dB SNR base acceleration signals in experiment (a,b) with simulated counterpart (c,d). The left column shows the fft of the input motions when normalized by the driving harmonic frequency. The right columns shows exemplary characteristics of the excitations in the time domain.

bandpass filtered motion (quasi-monochromatic noise [41]). Indeed, the structural/material damping capacity of trees, which are proposed to exploit 1:2 internal resonance, is apparently effective although the exciting vibrations are oftentimes largely composed of stochastic perturbations, showing that the nonlinear phenomena in this context are robust. The question as to the robustness of maintaining the saturation phenomenon for power generation enhancements in the internally-resonant, L-shaped energy harvesting platform is the focus of the following section.

6. Performance under harmonic and stochastic excitations

A common measure of robustness in energy harvesting systems is the "broadness" of the band of frequencies around which large amplitude dynamics are produced corresponding to high power generation [15]. Yet, as described in the previous paragraph, a more encompassing assessment of the effectiveness of an energy harvesting platform may be acquired by considering both the deviation in harmonic excitation frequency from a desired operating state *and* the deviation of the harmonic driving motions due to additive noise effects. This is the scope of the following investigation.

In the model, via Eq. (4), the pure harmonic base acceleration is corrupted with a zero-mean white noise $n_a(\tau)$. This study considers a range of *SNR* values from −6 dB to +6 dB, which means that the standard deviation of the white noise in a given simulation may be from 6 dB greater than to 6 dB less than the amplitude of the harmonic exciting motions, respectively. To clearly illustrate this feature, Fig. 6 shows the case for which the −6 dB *SNR* level of white noise (the greatest here evaluated) is added to the harmonic base acceleration at a frequency near ω_2. The top row presents the experimental version of the combined input form showing that the *mean* background noise amplitude is only about 1.5 orders of magnitude less than the pure harmonic response. A portion of the time series in Fig. 6(b) shows that the purity of the harmonic is strongly corrupted. The corresponding simulated version of this input motion is shown in the bottom row of plots and agrees qualitatively very well with the experimental realization of the harmonic and stochastic excitation combination. Such a distorted base acceleration is representative of ambient oscillations in which, for example, a structure (to harvest energy from) vibrates around well-known natural frequencies but has a persistent stochastic response added to the otherwise periodic behaviors. One particular example is a foot-bridge which oscillates in its low order natural frequency but is excited due to a collection of near-randomly distributed (in time and space) impulses [42]. For an L-shaped energy harvester attached to the foot-bridge, the motions of the foot-bridge are the net excitation resource and thus include both harmonic and stochastic components.

The robustness of activating the saturation phenomenon of the energy harvester due to this combined excitation form, and using the design parameters provided in Table 1, is first examined in Fig. 7. Throughout the figure, the steady-state results for pure harmonic excitation are shown as curves, where the dashed and solid curve styles denote dynamics proportional to the excitation frequency Ω and those proportional to half of that frequency $\Omega/2$, respectively. Symbols indicate results of the corresponding response amplitudes when various white noise levels are added to the harmonic base acceleration; each symbol denotes the findings for some noise level within the range of –6 dB to +6 dB *SNR* since many cases were evaluated for each selection of harmonic excitation conditions. It is important to note that while the experimental measurements of pure harmonic, steady-state excitations are evaluated using very slow parameter sweeps (in excitation amplitude or frequency), the experiments with the additive white noise are conducted without parameter sweeping. Instead, 60 second intervals are recorded for a prescribed set of excitation parameters (amplitude and frequency), then the level of white noise is changed and the process is repeated until a sufficient number of noise levels are taken into account.

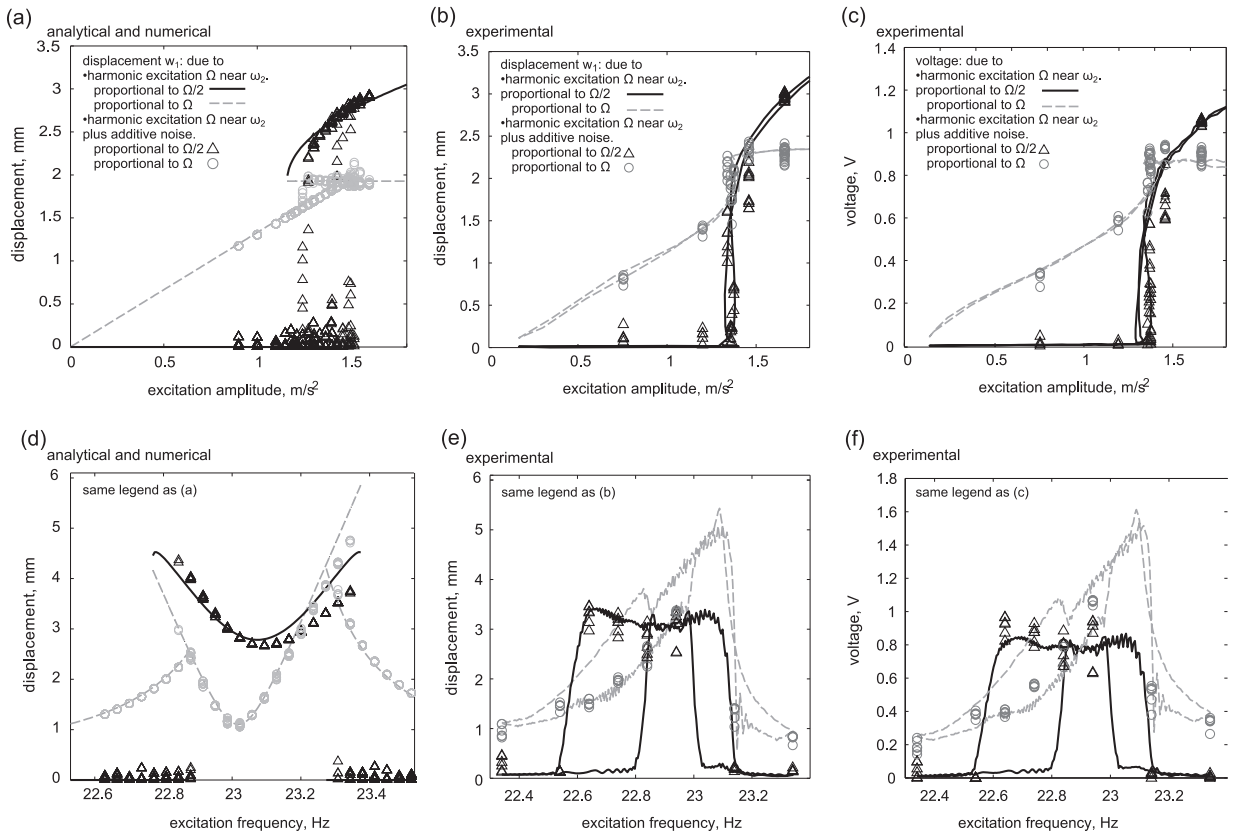

Fig. 7. Responses of the L-shaped energy harvester having parameters in Table 1. Top row, sensitivity of change in excitation acceleration amplitude on activating saturation at 22.89 Hz; bottom row, sensitivity of change in frequency of the harmonic base acceleration when the harmonic amplitude is 2.33 m/s^2. Left column, model results of the primary beam-mass structure displacement amplitudes. Middle column, corresponding measurements of the harvester primary structure displacements. Right column, corresponding experimental results of the transduced voltage as measured across a 5.4 MΩ resistor. In all plots, curves denote results for pure harmonic excitation while the circle and triangle points indicate responses due to combined harmonic and noise excitations.

Then, the excitation parameter of interest (whether excitation amplitude or frequency) is modified to a new value, and the procedure repeats once more.

The left column of Fig. 7 shows the analytical and numerical results in terms of the displacements of the primary beam-mass structure of the L-shaped harvester. Although the analytical model formulation using pure harmonic excitation predicts both stable and unstable responses [26], only the stable results are presented as the curves. The data points in the left column are those primary structural displacements determined from simulations including the various levels of additive white noise. The middle column shows the corresponding experimental measurements of the same sub-structural displacement, while the right column plots are the experimental measurements of the voltage as measured across a 5.4 MΩ resistor connected to the piezoelectric PVDF electrodes. Lastly, the top row shows the dependence of change in harmonic base acceleration amplitude when the frequency is 22.89 Hz, while the bottom row shows how the change in excitation frequency influences the trends when the amplitude of harmonic excitation is 2.33 m/s^2.

It is first observed that there is reasonable quantitative agreement between the corresponding values of primary structure displacements, comparing the left and middle columns of modeled and measured results, respectively. There is also good agreement with respect to the excitation parameters required to activate the saturation phenomenon. It is found that the frequencies of sensitivity deviated by approximately 0.2 Hz between analytical predictions and the experimental findings, which is apparent in the frequency axis of the plots on the bottom row of Fig. 7. Following a close examination of the experimental system, it is likely that this deviation is explained by a small rotational compliance in the clamped ends of the experimental system which is not accounted for in the model.

Fig. 7(a–c) show that the success of triggering saturation in the presence of additional stochastic excitations is notably more affected when the amplitude of the harmonic excitation is only slightly sufficient to active the phenomenon in the steady-state case. Thus, when noise corrupts the otherwise harmonic excitation, the existence of one critical excitation level or frequency to activate saturation is less accurate of a term as compared to a critical range of values. Within this range, Fig. 7(a–c) show that the resulting displacement and voltage amplitudes may not achieve the same magnitudes as those which occur under pure steady-state harmonic excitations. Because there is a narrow span of excitation amplitudes for

which a coexistence of the linear and nonlinear dynamic regimes occur, this critical range of activating the useful nonlinear, saturation-based responses becomes a practical concern since the additional noise reduces the assurance of one regime being sustained more than another. But for amplitudes of harmonic base acceleration above this critical range, the system indeed captures and sustains the saturated dynamics in spite of high levels of additive white noise, thus yielding an enhancement of generated power as shown in Fig. 2. In fact, once the saturated dynamic regime is activated, the resulting amplitudes of primary structure displacement and transduced voltage are not significantly different than those values determined for the ideal pure steady-state excitations.

The analytical and experimental findings for the influence of changing excitation frequency using a harmonic base acceleration amplitude of 2.33 m/s^2, shown in Fig. 7(d–f), provide another perspective. Under these conditions, the numerical and experimental findings agree that the ability of the L-shaped energy harvesting platform to obtain saturated dynamics is compromised for excitation frequencies near to the minimum and maximum frequencies which otherwise induce saturation for steady-state excitations. At these extremes of frequency, both results likewise agree that the mean amplitudes of the displacement and voltage responses may be more greatly impacted, although not necessarily adversely. For instance, at the lower frequency extent of the saturated dynamics, the numerical results in Fig. 7(d) around 22.8 Hz predict that the amplitude of the response proportional to $\Omega/2 \approx \omega_1$ may actually be greater than the steady-state value, and the experimental measurements of the transduced voltage from the energy harvester, Fig. 7(f) around 22.6 Hz, agree with this finding. In terms of robustness, the predicted and measured findings of Fig. 7 agree that the inducement of large amplitude, saturation-based dynamics for enhancing power generation from the L-shaped energy harvester is strongly affected by the additive white noise only in the excitation parameter regimes that correspond to the initial onset of saturation. Outside of this regime, the mean dynamical amplitudes do not substantially deviate from those values determined under pure harmonic excitations.

The prior design of the energy harvester yielded a 2.009 ratio of second to first natural frequencies. While this is close to the 1:2 internal resonance condition, a second design was realized by modifying mass and clamping positions to assess if a meaningful improvement in the voltage generation could be induced via a more ideal design. Table 2 provides the parameters of the L-shaped energy harvester once the design was modified so as to yield a 1.998 ratio of second to first natural frequencies. Fig. 8 shows the corresponding results acquired from the analytical, numerical, and experimental investigations. The top and bottom rows plot the findings for the changes in harmonic base acceleration amplitude and frequency, respectively. The plotting conventions used in Fig. 7 are likewise used in Fig. 8: curves indicate steady-state results (whether analytical or experimental) and the data points indicate results determined with the additive white noise excitations of various *SNR* values (whether numerical or experimental).

Like the results presented in Fig. 7, in Fig. 8(a,b) and (d,e) there are good quantitative agreements between the analytical and numerical results with the corresponding measured values of the displacement amplitude of the primary beam-mass sub-structure, giving confidence in the analytical formulation as a useful predictive tool for future investigations of these energy harvesting platforms. Fig. 8(a–c) indicate that the onset of the saturation phenomenon occurs at lower levels of the harmonic base acceleration when the ratio of the natural frequencies more closely achieves the ideal 1:2 condition. The predictions and measurements are in good agreement regarding this trend. In addition, the span of harmonic acceleration amplitudes which lead to coexisting dynamics is greatly reduced for this frequency of excitation, Fig. 8(a–c); in fact, there is no coexistence identified for the steady-state excitation condition. For energy harvesting applications, the increased likelihood of obtaining one dynamical regime or the other is preferred, since it provides for a more effective assurance of power generation under a prescribed excitation amplitude and frequency. Fig. 8(a–c) also show that high levels of additive white noise lead to a more diffused parameter regime of excitation amplitudes which ultimately trigger the useful saturated dynamics. Yet, similar to the findings in Fig. 7(a–c), Fig. 8(a–c) reveal that the presence of the white noise does not appreciably change the resulting displacement and voltage amplitudes of the L-shaped energy harvester from the steady-state result when the base acceleration level is greater than the critical range that initially triggers saturation.

The frequency dependence of activating saturation in the modified design of the energy harvester is assessed in Fig. 8(d, e,f) when the amplitude of harmonic excitation is 2.33 m/s^2, the same level as employed for the initial design. While the analytical and numerical data in Fig. 8(d) agree that a relatively broad bandwidth of frequencies assures the achievement of beneficial saturated dynamics, the slowly swept experimental results for “steady-state” excitations in Fig. 8(e,f) (curves) are seen to maintain the linear dynamic regime over a much wider range of frequencies. It is likely that this deviation is due to the frequency sweep experimentation strategy for the pure harmonic excitations, since the onset of bifurcations is sensitive to non-stationary parameter change [43]. This hypothesis is strongly supported by the experimental measurements conducted using a fixed frequency of harmonic excitation with additive white noise because these results exhibit a relatively broad bandwidth of frequencies across which only the large amplitude, saturated dynamics were triggered, which is in very good agreement with the model predictions. Both the numerical results and the measurements in Fig. 8(d–f), respectively, also concur that the full extent of frequencies to trigger saturation is reduced when the stochastic noise corrupts the harmonic base acceleration signal; this is a similar trend as that uncovered via Fig. 7(d–f).

It is apparent that the more ideal frequency ratio, $\omega_2/\omega_1 = 1.998$, does indeed lead to greater amplitudes of transduced voltage for the same harmonic excitation level, as well as an increased symmetry in terms of the dependence upon the excitation frequency, shown in Fig. 8(d–f). The latter feature of symmetry is practically important because the unavoidable change in excitation frequency from an initial operating state “centered” in the saturated frequency bandwidth will cause the same change in voltage amplitude, whether the frequency shift is increasing or decreasing. In contrast, nonlinear

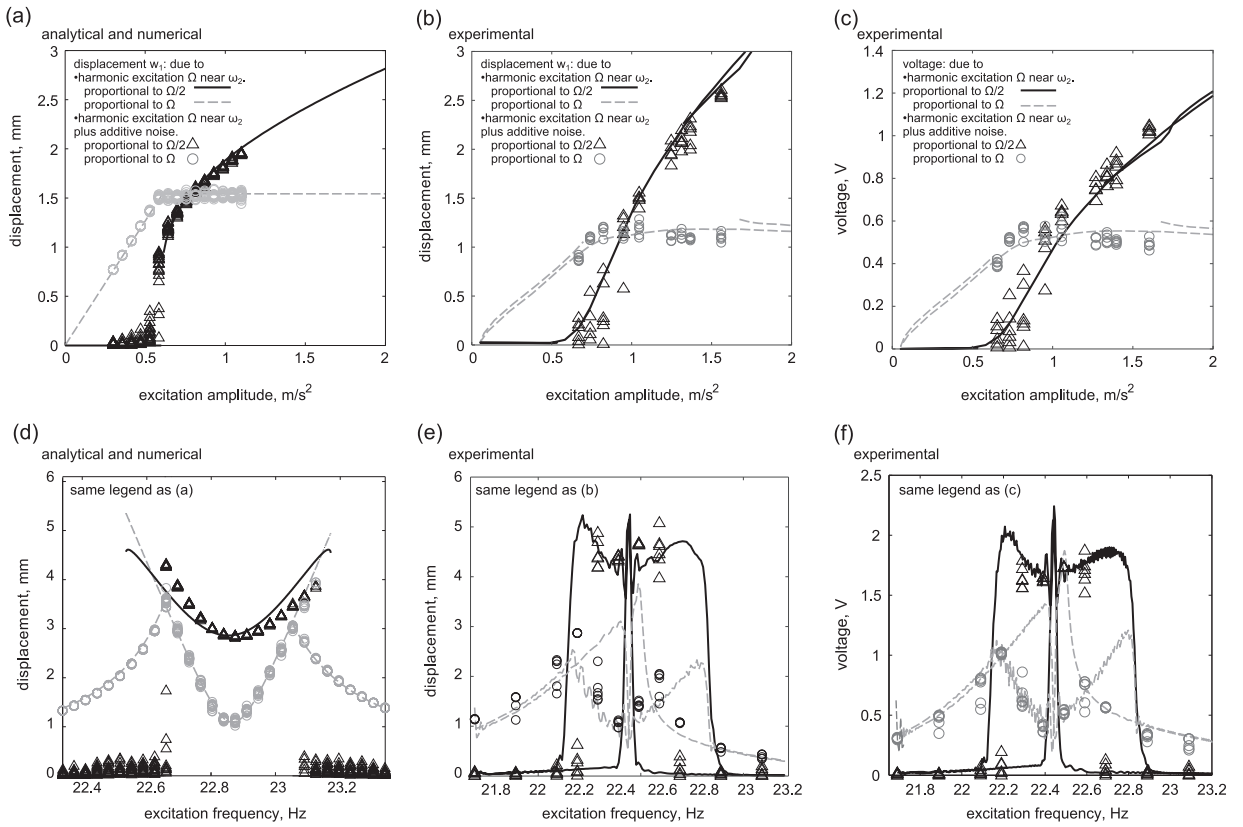

Fig. 8. Responses of the L-shaped energy harvester having parameters in Table 2. Top row, sensitivity of change in excitation acceleration amplitude on activating saturation at 22.27 Hz; bottom row, sensitivity of change in frequency of the harmonic base acceleration when the harmonic amplitude is 2.33 m/s^2. Left column, model results of the primary beam-mass structure displacement amplitudes. Middle column, corresponding measurements of the harvester primary structure displacements. Right column, corresponding experimental results of the transduced voltage as measured across a 5.4 MΩ resistor. In all plots, curves denote results for pure harmonic excitation while the circle and triangle points indicate responses due to combined harmonic and noise excitations.

phenomena like those in Duffing or bistable energy harvester platforms do not exhibit symmetry in terms their response variation for a given increase/decrease in excitation frequency [14,15], which means that adverse and poor-performing operating states may result when the frequency deviates from the ideal, initial condition. In fact, Fig. 8(e,f) reveal that deviation from the center frequency of the saturation bandwidth only results in an increase in the voltage amplitudes of the L-shaped energy harvester, up until the point at which the frequency deviates so much that the saturated dynamics are no longer sustainable.

7. Discussion and conclusions

Following a complementary set of insights that internal resonance-based phenomena are useful as robust damping mechanisms to sustain trees under wide-ranging excitation conditions, this research sought to answer three important questions related to the strategic exploitation of saturation-based dynamics in the L-shaped energy harvester platform.

The first question was whether there is genuinely a justification for this goal because internal resonance-induced saturation overall *reduces* the primary frequency of steady-state vibration of the energy harvester whereas the transduced voltage amplitude is directly proportional to the excitation frequency (hence, average power is proportional to the frequency squared) [2]. Thus, if coexisting dynamics occur including a linear regime with all vibration at frequency $\Omega \approx \omega_2$ and a saturated, nonlinear regime with vibration diffused between frequencies $\Omega \approx \omega_2$ and $\Omega/2 \approx \omega_1$, will the saturated dynamics lead to an increase in average electric power generation? In fact, as Figs. 2 and 3 reveal, there is plainly an enhancement of average power when the saturated responses are triggered. In both cases, the power increase was more than two times and similar or greater enhancement is computed via the steady-state experimental results in Figs. 7 and 8(c,f). The considerably large amplitudes of motion which are triggered at a frequency $\Omega/2 \approx \omega_1$ are the source of the power enhancement. A related and practical consequence is that the particular diffusion of the harmonic energy from $\Omega \approx \omega_2$ to $\Omega/2 \approx \omega_1$ may require special charging and storage power electronics that intelligently determine when to transition an AC–DC conversion strategy from switching at Ω to switching at $\Omega/2$ for best performance [44].

The second question was motivated by historical works on internal resonance and saturation which suggested that the range of pure harmonic excitation frequencies and design parameters inducing saturation might be constrained in their breadth for the L-shaped structure. Thus, would a more refined assessment of the sensitivities confirm this initial insight or uncover new perspectives? Indeed, Figs. 4 and 5 confirm this early insight, and the corresponding experimental measurements throughout this research likewise reveal that small changes in the harmonic excitation frequency and design parameters may significantly influence the potential for triggering the saturation-based dynamics useful for energy harvesting performance enhancement. Therefore, to effectively exploit the L-shaped energy harvester and the saturation-based dynamics, it is clear that the application must provide sufficiently stationary harmonic excitation properties and the electroelastic design composition of the platform must achieve considerable accuracy with respect to an ideal parameter set. The achievement of such ideal characteristics is entirely application-dependent, so broad generalizations as to the likelihood of obtaining the preferred characteristics are not practically possible.

The final question began from the assumption that an ideal, harmonic vibration resource is available, but the net ambient excitations are appreciably corrupted with additional non-deterministic motions. An example ambient vibration resource comparable to this scenario might be a foot-bridge which oscillates freely in a low order natural frequency due to a randomly distributed supply of impulsive walking motions that moreover induce some proportion of stochastic vibrations. Application of the L-shaped energy harvester to such a foot-bridge then excites the attached device with combined harmonic and stochastic inputs. Thus, this research has sought to answer: what is the impact of additive white noise on the achievement of large amplitude dynamics associated with internal resonance and saturation in the L-shaped harvester system? From the results presented in Figs. 7 and 8, it may be concluded that while activating saturation-based dynamics in the critical regimes of its initial onset is sensitive to stochastic perturbations, even very large additive noise levels have little or no influence on the mean values of transduced voltage from the energy harvester when the harmonic excitation conditions are removed from the critical regime of possible dynamic coexistence. So long as the coexistence of the linear and nonlinear dynamic regimes is eliminated under the corresponding case of steady-state excitations, the experimental measurements and analytical predictions found that no amount of white noise could inhibit the L-shaped energy harvester from realizing the large amplitude saturation-based dynamics. This finding is attributed to the related study of necessary and sufficient conditions to trigger dynamic bifurcations [45,46]: if such conditions are satisfied and no other steady-state attractors occur, additional influences will only lead to deviations around the stable attractor(s) rather than cause a deterioration of the attractor towards an entirely different dynamic steady-state.

In summary, the L-shaped vibration energy harvesting platform is an effective system with which to exploit the 1:2 internal resonance and saturation for improving the energy conversion performance under sufficiently constant harmonic excitation conditions, even if the input vibrations include a high level of additive white noise. The findings of this research also serve as more general evidence that particular nonlinear dynamic phenomena may provide a robust capacity for energy dissipation (whether dampened by electromechanical influences in the harvester beam and storage circuit, or materially dampened in the branches of a tree) even when the exciting vibrations deviate substantially from pure harmonic motions. Other saturation-based harvester platforms may likewise exhibit such robustness to additive stochastic perturbations and other systems may also improve upon the potentially limiting design- and excitation-based sensitivities of the L-shaped platform. Finally, the findings of this work therefore serve as motivation for future studies on the exploitation of internal resonance and saturation for broadening the usefulness of vibration-based energy harvesting systems.

Acknowledgments

This research is supported by the University of Michigan Summer Undergraduate Research in Engineering (SURE) program, and by the University of Michigan Collegiate Professorship.

References

[1] H.A. Sodano, D.J. Inman, G. Park, A review of power harvesting from vibration using piezoelectric materials, *Shock Vib. Dig.* 36 (2004) 197–205.
[2] A. Erturk, D.J. Inman, *Piezoelectric Energy*, Harvesting, Wiley, Chichester, 2011.
[3] N. Elvin, A. Erturk, *Advances in Energy Harvesting Methods*, Springer, New York, 2013.
[4] L. Zuo, X. Tang, Large-scale vibration energy harvesting, *J. Intell. Mater. Syst. Struct.* 24 (2013) 1405–1430.
[5] T. Speck, I. Burgert, Plant stems: functional design and mechanics, *Annu. Rev. Mater. Res.* 41 (2011) 169–193.
[6] J.R. Moore, A.D. Maguire, Natural sway frequencies and damping ratios of trees: concepts, review and synthesis of previous studies, *Trees* 18 (2004) 195–203.
[7] L.A. Miller, Structural dynamics and resonance in plants with nonlinear stiffness, *J. Theor. Biol.* 234 (2005) 511–524.
[8] H.C. Spatz, F. Brüchert, J. Pfisterer, Multiple resonance damping or how do trees escape dangerously large oscillations? *Am. J. Bot.* 94 (2007) 1603–1611.
[9] M. Rodriguez, E. De Langre, B. Moulia, A scaling law for the effects of architecture and allometry on tree vibration modes suggests a biological tuning to modal compartmentalization, *Am. J. Bot.* 95 (2008) 1523–1537.
[10] M. Rodriguez, S. Ploquin, B. Moulia, E. de Langre, The multimodal dynamics of a walnut tree: experiments and models, *J. Appl. Mech.* 79 (2012) 044505.
[11] B. Theckes, E. de Langre, X. Boutillon, Damping by branching: a bioinspiration from trees, *Bioinspir. Biomim.* 6 (2011) 046010.
[12] H.C. Spatz, B. Theckes, Oscillation damping in trees, *Plant Sci.* 207 (2013) 66–71.
[13] L. Tang, Y. Yang, C.K. Soh, Toward broadband vibration-based energy harvesting, *J. Intell. Mater. Syst. Struct.* 21 (2010) 1867–1897.
[14] R.L. Harne, K.W. Wang, A review of the recent research on vibration energy harvesting via bistable systems, *Smart Mater. Struct.* 22 (2013) 023001.

[15] M.F. Daqaq, R. Masana, A. Erturk, D.D. Quinn, On the role of nonlinearities in vibratory energy harvesting: a critical review and discussion, *Appl. Mech. Rev.* 66 (2014) 040801.
[16] H. Wu, L. Tang, Y. Yang, C.K. Soh, Development of a broadband nonlinear two-degree-of-freedom piezoelectric energy harvester, *J. Intell. Mater. Syst. Struct.* 25 (2014) 1875–1889.
[17] R.L. Harne, M. Thota, K.W. Wang, Bistable energy harvesting enhancement with an auxiliary linear oscillator, *Smart Mater. Struct.* 22 (2013) 125028.
[18] Z. Wu, R.L. Harne, K.W. Wang, Energy harvester synthesis via coupled linear-bistable system with multistable dynamics, *J. Appl. Mech.* 81 (2014) 061005.
[19] G. Litak, Energy harvesting by coupled oscillators forced by excitations with harmonic and random components, *Proc. Appl. Math. Mech.* 14 (2014) 289–290.
[20] H. Karimpour, M. Eftekhari, Exploiting internal resonance for vibration suppression and energy harvesting from structures using an inner mounted oscillator, *Nonlinear Dyn.* 77 (2014) 699–727.
[21] L.Q. Chen, W.A. Jiang, An electromagnetic energy harvester based on internal resonance, in: Proceedings of the 17th U.S. National Congress on Theoretical and Applied Mechanics, East Lansing, Michigan, USA, 2014, pp. D-12–972.
[22] G. Gatti, M.J. Brennan, I. Kovacic, On the interaction of the responses at the resonance frequencies of a nonlinear two degrees-of-freedom system, *Phys. D: Nonlinear Phenom.* 239 (2010) 591–599.
[23] K. Yang, R.L. Harne, K.W. Wang, H. Huang, Dynamic stabilization of a bistable suspension system attached to a flexible host structure for operational safety enhancement, *J. Sound. Vib.* 333 (2014) 6651–6661.
[24] Z. Lu, T. Yang, M.J. Brennan, X. Li, Z. Liu, An investigation into the isolation performance of mono- and bi-stable systems, *J. Mar. Sci. Appl.* 13 (2014) 291–298.
[25] R.L. Harne, K.W. Wang, A bifurcation-based coupled linear-bistable system for microscale mass sensing, *J. Sound. Vib.* 333 (2014) 2241–2252.
[26] A.G. Haddow, A.D.S. Barr, D.T. Mook, Theoretical and experimental study of modal interaction in a two-degree-of-freedom structure, *J. Sound. Vib.* 97 (1984) 451–473.
[27] B. Balachandran, A.H. Nayfeh, Nonlinear motions of beam-mass structure, *Nonlinear Dyn.* 1 (1990) 39–61.
[28] S.L. Bux, J.W. Roberts, Non-linear vibratory interactions in systems of coupled beams, *J. Sound. Vib.* 104 (1986) 497–520.
[29] E. de Langre, Effects of wind on plants, *Annu. Rev. Fluid Mech.* 40 (2008) 141–168.
[30] J.W. Roberts, Random excitation of a vibratory system with autoparametric interaction, *J. Sound. Vib.* 69 (1980) 101–116.
[31] R.A. Ibrahim, J.W. Roberts, Broad band random excitation of a two-degree-of-freedom system with autoparametric coupling, *J. Sound. Vib.* 44 (1976) 335–346.
[32] R.A. Ibrahim, Y.J. Yoon, M.G. Evans, Random excitation of nonlinear coupled oscillators, *Nonlinear Dyn.* 1 (1990) 91–116.
[33] A. Erturk, J.M. Renno, D.J. Inman, Modeling of piezoelectric energy harvesting from an L-shaped beam-mass structure with an application to UAVs, *J. Intell. Mater. Syst. Struct.* 20 (2009) 529–544.
[34] R.A. Ibrahim, Excitation-induced stability and phase transition: a review, *J. Vib. Control* 12 (10) (2006) 1093–1170.
[35] J.F. Rhoads, S.W. Shaw, K.L. Turner, Nonlinear response of resonant microbeam systems with purely-parametric electrostatic actuation, *J. Micromech. Microeng.* 16 (2006) 890–899.
[36] A.H. Nayfeh, D.T. Mook, *Nonlinear Oscillations*, Wiley, Weinheim, 1995.
[37] P.R. Sethna, Steady-state undamped vibrations of a class of nonlinear discrete systems, *J. Appl. Mech.* 27 (1960) 187–195.
[38] N.E. DuToit, B.L. Wardle, S.G. Kim, Design considerations for MEMS-scale piezoelectric mechanical vibration energy harvesters, *Integr. Ferroelectr.* 71 (2005) 121–160.
[39] A.H. Nayfeh, B. Balachandran, M.A. Colbert, M.A. Nayfeh, An experimental investigation of complicated responses of a two-degree-of-freedom structure, *J. Appl. Mech.* 56 (1989) 960–967.
[40] S.S. Rao, *Mechanical Vibrations*, 4th ed. Pearson Prentice Hall, Upper Saddle River, New Jersey, 2004.
[41] M. Dykman, K. Lindenberg, Fluctuations in nonlinear systems driven by colored noise, in: G.H. Weiss (Ed.), *Contemporary Problems in Statistical Physics*, SIAM, Philadelphia, 1994.
[42] P.L. Green, E. Papatheou, N.D. Sims, Energy harvesting from human motion and bridge vibrations: an evaluation of current nonlinear energy harvesting solutions, *J. Intell. Mater. Syst. Struct.* 24 (2013) 1494–1505.
[43] E. Benoît, *Dynamics Bifurcations*, Springer-Verlag, Berlin, 1991.
[44] Y.C. Shu, I.C. Lien, W.J. Wu, An improved analysis of the SSHI interface in piezoelectric energy harvesting, *Smart Mater. Struct.* 16 (2007) 2253–2264.
[45] J. Guckenheimer, P.J. Holmes, *Nonlinear Oscillations, Dynamical Systems, and Bifurcations of Vector Fields*, Springer, New York, 1983.
[46] S. Wiggins, *Introduction to Applied Nonlinear Dynamical Systems and Chaos*, Springer, New York, 2003.